Efficient Charging and Data Collection in UAV-Aided Backscatter Sensor Networks

Amit Goel, Nancy Varshney, and Swades De

Abstract

Backscatter communication based wireless charging of the sensor nodes and data collection from them is a promising solution due to ultra-low power consumption. However, challenges of short transmission range requirement, high self-interference, and simultaneous operation with multiple backscatter nodes (BSNs) need to be addressed. To this end, this paper presents a novel framework for joint field data collection and wireless charging in an unmanned aerial vehicle (UAV)-aided wireless sensor network via monostatic backscatter communication at millimeter waves. The framework is divided into three tasks, namely, energy-optimized UAV transceiver design, UAV constraints aware BSN clustering, and optimized resource allocation per cluster. To strike a balance between serving efficiency and self-interference, optimum BSN cluster size is estimated offline, which in turn governs BSN clustering optimization. With UAV communication energy and clustering information, a joint sum energy transfer and sum data collection maximization problem is formulated by considering the minimum required charging and data collection constraints. To handle non-convexity, an alternating optimization approach is devised, estimating optimal backscatter reflection coefficients, data collection time, and power distribution among the BSNs using successive convex approximation. Finally, via Monte-Carlo simulations, performance of the proposed system is compared with the current state-of-the-art.

Index Terms

Backscatter communication, wireless energy transfer, self-interference, energy efficiency, unmanned aerial vehicle (UAV)

I. INTRODUCTION

Recent advances in wireless technologies have enabled the vision of massive Internet of Things (IoT) network where billions of IoT sensor nodes monitor, communicate, and possibly control

The authors are with the Department of Electrical Engineering and Bharti School of Telecommunication, Indian Institute of Technology Delhi, New Delhi 110016, India.

the intended entities in different applications [1]. However, the scalability and flexibility of IoT sensor node deployment are limited by the communication medium, energy constraints, and network cost. Conventional IoT sensor nodes use batteries for sensing and communication. But their limited battery life necessitates frequent replacement or recharging, which can be costly and challenging in hazardous or inaccessible deployment areas. To address this challenge, technologies with near-zero communication power requirements, like backscatter communication (BSC), are being investigated.

A BSC system comprises backscatter tags, a carrier emitter, and a backscatter receiver. The backscatter tags transmit data by modulating and reflecting the incident radio frequency (RF) wave emitted by the carrier emitter toward the backscatter receiver. Backscatter tags, such as RF identification cards, are examples of passive devices that do not require a battery for data transfer. In contrast, as a sensor, a backscatter node (BSN) functions in a semi-passive mode with a small rechargeable battery to power its sensing activity [2]. Further, unmanned aerial vehicle (UAV) is being considered as a flexible option for on-demand energy supply through RF wireless energy transfer (WET) without incurring high infrastructure costs [3]. In addition, directional beams can enhance RF energy harvesting. Sub-6 GHz band operation limits the number of UAV-mounted antennas and results in broad beams. This limitation is addressed by utilizing millimeter-wave (mmWave) technology, enabling the deployment of large antenna arrays to generate highly directional beams [4]. When used in conjunction with UAVs, this further minimizes the spot size of the main lobe of the beam because of the short communication distance. It also establishes a strong line-of-sight communication link, leading to reduced interference between nodes in multi-node communication situations.

A. Related Work

The two broad BSC system configurations are monostatic BSC and bistatic BSC. In a monostatic BSC architecture the carrier emitter and BSC receiver are co-located, whereas in bistatic BSC they are physically separated. In [5], the authors presented a data collection framework for BSC networks, wherein a UAV-based bistatic BSC architecture with multiple terrestrial carrier emitters was considered to optimize the UAV energy efficiency. In remote or rural areas it is less likely to have high-density of terrestrial communication infrastructure [6]; hence for most applications UAV-aided monostatic BSC is preferred.

The authors in [7] studied two strategies for optimizing UAV operations during sensor data collection under limited energy availability: minimizing UAV flight duration and maximizing UAV energy efficiency. Meanwhile, the authors in [8] investigated network lifetime maximization aspects of UAV-aided sensor data collection. This study examined sensor nodes equipped with hybrid transmitters capable of switching between conventional wireless information transfer (WIT) and BSC phases to optimize network lifetime. In contrast to passive data transmission in BSC phase, a BSN acts as an active device during WIT phase, generating its own data signal utilizing its power. With every instance of sensing and data offloading, each BSN incurs an energy cost. Hence, for semi-passive BSNs energy is a crucial resource that must be utilized sparingly and replenished timely. The authors in [9] established closed-form expressions for the outage probability of a UAV-aided monostatic BSC system at sub-6 GHz. Considering two UAVs-aided systems for full duplex communication, the authors in [10] studied the resource allocation problem for maximizing throughput with two UAVs by deploying one UAV each for downlink and uplink data transmission. In BSC networks, WET occurs in downlink and WIT in uplink. Since WIT operations are followed by WET, segregating operations and allocating different UAVs would not be efficient.

It is worth noting that the authors in [8]–[10] optimized different parameters, namely, energy efficiency, power allocation, and node visiting sequence while serving a single BSN at a time. The study in [11] addressed the issue of serving multiple sensor nodes and introduced a strategy for joint location and power allocation in NOMA-UAV networks. In scenarios where sensor nodes are sparsely distributed, simultaneous servicing of all nodes becomes impractical, prompting the exploration of clustering as a more viable alternative. The study in [12] incorporated signal-to-noise ratio outage constraints to determine the cluster radius, while orthogonal frequency division multiplexing resource blocks govern the maximum number of users in a cluster. Similarly, in [13], considering a fixed amount of required energy to be harvested at each sensor node for energy sustainability, integrated WET strategy with UAV trajectory design was proposed at sub-6 GHz range. The study in [14] aimed at enhancing the system throughput of an underground BSC network for smart agriculture where a single beam-based BSC transceiver was employed for data collection from the BSNs via harvest-then-sequentially offload protocol (HTSeqOP).

The existing studies focused on optimizing monostatic BSC operation in sub-6 GHz range, where a broad beam covered all the BSNs within its coverage area. They optimized either BSN clustering [12] or beam coverage [13]. The most relevant work at mmWaves is [15] that considers

multiple beams in a UAV-based wireless-powered mobile edge computing system, but it does not consider BSC. Specifically, all IoT nodes harvest energy during the first phase and transmit data simultaneously using harvested energy in half-duplex communication mode, which we call harvest-then-simultaneous offload protocol (HTSimOP). This approach does not account for high power consumption of hardware as it uses the same number of RF chains as the number of served IoT sensor nodes for simultaneous energy and data transfer in uplink.

On energy harvesting modeling, coverage probability and transmission capacity of backscatter networks were studied in [16] by considering a linear energy harvesting model. However, experimental studies have shown that the energy harvesting circuitry exhibits non-linearity in practice. A more realistic non-linear energy harvesting model was proposed in [17], where the energy efficiency of multi-tag BSC networks was optimized using max-min based optimization.

B. Motivation

The reported research highlighted in [8]–[10], [16], [17] primarily focused on UAV-aided BSC for IoT data collection and WET. However, there is a need for further investigation into the energy efficiency of joint powering and data collection. In view of the limited onboard energy capacity of the UAVs, for effective charging and data collection, a UAV should minimize energy expenditure and intelligently allocate the increased power availability. Addressing this challenge requires a holistic approach, considering transceiver architecture design, UAV maneuverability, and resource allocation simultaneously.

Unlike the previous approaches [12], [13], leveraging the directionality of communication at mmWaves, the UAV can utilize multiple beams for simultaneous WET and BSC. From a transceiver architecture perspective, reducing hardware power consumption at mmWaves is a key concern that necessitates a decrease in RF chains without compromising the generation of multiple beams. On the other hand, while considering UAV maneuverability, determining the optimal combination of nodes to be served together and their visiting sequence is crucial. At a high altitude, serving all nodes in a single sweep may seem ideal. Yet, it becomes infeasible due to dual-channel path loss in backscatter communication and low energy harvesting efficiency. Moreover, increasing the number of beams to serve more BSNs simultaneously raises self-interference, which can reduce QoS. This aspect necessitates careful consideration of the number of BSNs to be served together to strike a balance between serving efficiency and self-interference. From a node perspective, BSN has two primary purposes: to sense and to transfer information. It

is necessary that minimum required energy and data rate are ensured while performing resource allocation. However, the challenge arises when BSNs may demand additional energy for increased frequent sensing or higher data rates essential for updating specific field status. Addressing this challenge entails formulating an optimization problem that concurrently optimizes weighted sum data rate and energy harvesting. This is essential for adapting to dynamic demands in BSNs across different spatio-temporal conditions while maintaining a minimum threshold fairness among BSNs.

Based on our literature studies, as presented above, there is a research gap in the literature regarding the exploration of efficient UAV transceiver architecture with low-power RF circuitry and resource allocation strategy for joint data collection and wireless charging of multiple BSNs. This research aims to fill this gap and contribute to the understanding of efficient UAV-aided BSC for IoT applications.

C. Contributions and Scope

To address the research gap on efficient data collection and energy sustainability of field sensor nodes, we propose a novel multi-beam UAV-aided monostatic BSC system at mmWaves that takes into account critical system aspects. The key contributions of this work are summarized as follows.

1) A novel UAV-aided monostatic BSC and WET system is proposed for joint charging of BSNs and data collection from them using multiple directional beams at mmWaves. This architecture requires only three RF chains at the UAV to generate multiple beams, with each beam targeting a single BSN within a cluster. The resulting residual self-interference (RSI) on the data beam at the UAV receiver from simultaneously active energy beams is addressed in the achievable system performance.
2) An optimal number of beams is estimated offline for the proposed UAV transceiver architecture to maximize energy efficiency, allowing to determine the optimal number of BSNs per cluster to be served simultaneously.
3) For a system with a total number of BSNs larger than the number of beams supported at the UAV, BSN clustering is performed based on beam steering constraints and the optimal number of beams estimated offline. Thereafter, BSN cluster visiting sequence is also determined.

4) For joint BSC and WET operation, an optimization problem is formulated considering the minimum BSN energy harvesting and data rate constraints as well as UAV power limit. Due to inter-dependency of the optimization variables, the problem is non-convex. An alternating optimization technique is devised that iteratively estimates power allocation among the beams, reflection coefficients, and data collection time for each BSN in a cluster.
5) Finally, through extensive Monte Carlo simulations, the proposed system model's performance is compared with the existing state-of-the-art approaches.

While our current study considers a single UAV, there is potential for improving time-constrained operations via multi-UAV cooperation, which is out of scope of this study.

The proposed UAV-aided monostatic BSC and WET system model is presented in Section II, followed by the overall problem formulation and resource allocation optimization in Section III. Complexity and convergence analysis is presented in Section IV. Simulation results are discussed in Section V, and concluding remarks are drawn in Section VI.

II. Proposed System Model

This section presents the proposed BSC and WET system architecture and modeling of the various parameters associated with the working of UAV-aided BSC and WET system.

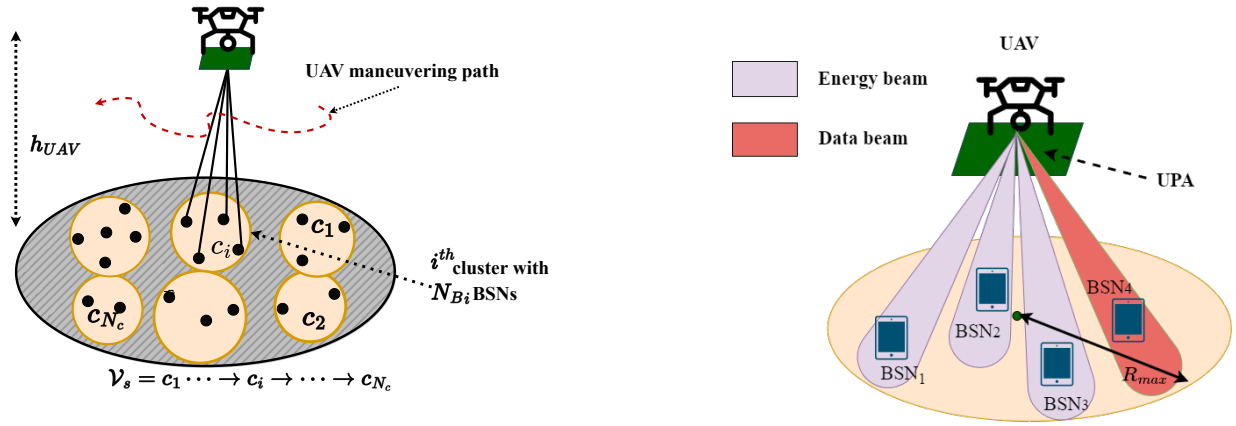

(a) (b)

Figure 1: (a) Illustration of N BSNs, grouped into N_c clusters with N_{Bi} BSNs in i^{th} cluster being served by the UAV according to cluster visiting sequence $\mathcal{V}_s$. (b) UAV serving i^{th} having $N_{Bi} = 4$ BSNs with a total $N_B = 4(= N_{Bi})$ beams.

Table I: System parameters and their notations

Notation	Description	Notation	Description
D_{th}	Minimum data collection requirement	v_o	Mean induced velocity in hovering
E_{th}	Minimum energy harvesting requirement	s	Rotor solidity
P_{BSN}	BSN internal circuitry power consumption	A	Area of rotor disk
$D_{\tau,i,k}$	Data offloaded by k^{th} BSN of i^{th} cluster in τ^{th} interval	Ω	Blade angular velocity
$E_{\tau,i,k}$	Energy harvested by k^{th} BSN of i^{th} cluster in τ^{th} interval	R	Rotor radius
$\beta_{\tau,i,k}$	Reflection coefficient to k^{th} BSN of i^{th} cluster in τ^{th} interval	W	Weight of UAV
ς_1, ς_2	scaling weights	ρ	Density of air
η_{PA}	Efficiency of power amplifier	U_{tip}	Tip speed of rotor blade
P_{LNA}	Power consumption of low noise amplifier	V	UAV velocity while maneuvering
P_{M}	Power consumption of mixer	d_o	Fuse large drag ratio
P_{O}	Power consumption of local oscillator	$\mathcal{V}_s$	Cluster visiting sequence
P_{LPF}	Power consumption of low pass filter	δ	Profile drag coefficient
P_{DAC}	Power consumption of digital-to-analog converter	N_{Bi}	Number of BSNs in i^{th} cluster
P_{ADC}	Power consumption of analog-to-digital converter	N_B^*	Optimal number of beams
k_e	Incremental correction factor to induced power	N_c	Number of clusters

A. Proposed System Architecture and Operation Protocol

We consider a UAV-aided monostatic BSC and WET system at mmWaves with N BSNs distributed according to a Binomial point process across a two-dimensional (2D) circular region of radius R_{AOI}, as shown in Fig. 1(a). Rotary wing UAV is considered to serve the BSNs, owing to its ability to hover stably and move around at low altitudes. The UAV is equipped with a uniform planar array (UPA) of antenna elements capable of generating maximum N_B^{max} directional beams, with each beam generated from a subarray comprising $N_T{=}N_x \times N_y$ antenna elements. Each BSN is equipped with a single antenna. Let, $\mathcal{X}_k{=}\{x_k, y_k, z_k\}$ and $\mathcal{X}_v{=}\{x_v, y_v, z_v\}$ denote the Cartesian coordinates of the k^{th} BSN and UAV, respectively. We assume that $N_B^{max} \ll N$ and hence BSNs are clustered into N_c clusters, each containing $N_{Bi} \leq N_B^{max}$ BSNs in i^{th} cluster, so that $\cup_{i=1}^{N_c} |N_{Bi}| {=} N$. The UAV serves the i^{th} cluster of N_{Bi} BSNs while generating a total of those many number of beams for a hovering duration of T_h, after which it moves to the next cluster, based on the cluster visiting sequence $\mathcal{V}_s$. The UAV is considered to hover at a height $z_v{=}h_{\text{UAV}}$ at the center of a cluster. Additionally, we assume constant hovering time T_h for all clusters, regardless of the value of N_{Bi}. Furthermore, T_h is divided into $\tau_{tot}{=}\lfloor T_h/t_c \rfloor$ intervals each of time period t_c, where t_c denotes the coherence time. The time intervals are indexed by $\tau \in \{1, 2, \cdots, \tau_{tot}\}$.

In beginning of every interval a small fraction of time is utilized for channel estimation and synchronization and in the rest of the time BSC and WET operations are performed [5].

The backscatter nodes (BSNs) are static and deployed in remote geographical locations. As the UAV serves these nodes while hovering and maintaining a stationary position, any significant movement during service is avoided. Additionally, the short communication range and high probability of line-of-sight contribute to minimal fading effects. Furthermore, as the studies in [18], [19] demonstrated, narrow beam and directional transmission reduce the channel state information (CSI) variation, facilitating longer coherence time and reasonably accurate CSI estimation [20]. We use time division multiple access to serve BSNs within a cluster, dividing the τ^{th} interval into N_{Bi} slots. During each slot, one beam collects data from a specific BSN while the others transmit energy to the remaining BSNs in the cluster. The duration of the k^{th} slot is denoted by $t_{\tau,i,k}$. In each subsequent slot, data is collected from a different BSN while the others harvest energy. For example, as shown in Fig. 2 (a), consider a $N_{Bi} \times N_{Bi}$ matrix to represent the time instants and BSN's operations in the τ^{th} interval of i^{th} cluster. Therefore, at a given time only one BSN operates in BSC mode to transmit data while the remaining BSNs harvest energy from the energy beams. In addition to reducing the number of the RF chains in the UAV (as discussed next in Section II-B), only one BSN is allowed to operate in BSC mode to reduce co-backscatter node interference. However, the UAV's residual self-interference remains intact due to the presence of energy beams.

B. Proposed Transceiver Architecture

We propose a novel energy-efficient UAV transceiver architecture that enables joint operation of simultaneous backscatter-based data collection and energy transfer to multiple BSNs. The UAV transmitter RF front-end is composed of only three RF chains coupled to an antenna array that can generate maximum N_B^{max} directional beams (Fig. 2(b)). The first RF unit, RF_1 generates an amplified carrier signal that is transmitted via multiple beams, called energy beams, to charge the BSNs. While serving the i^{th} cluster, $N_{Bi}-1$ energy beams are generated by $N_{Bi}-1$ non-overlapping antenna subarrays of size $N_x \times N_y$ connected to RF_1 via power splitters and phase shifters. These components are controlled by a digital signal processor [21] to steer the beams and divide power suitably among them. Notably, since the energy beams do not require different digital modulations, they can all be managed by a single RF chain. The other two RF chains, RF_2 and RF_3, enable full-duplex BSC operation to collect data from a BSN. They are connected

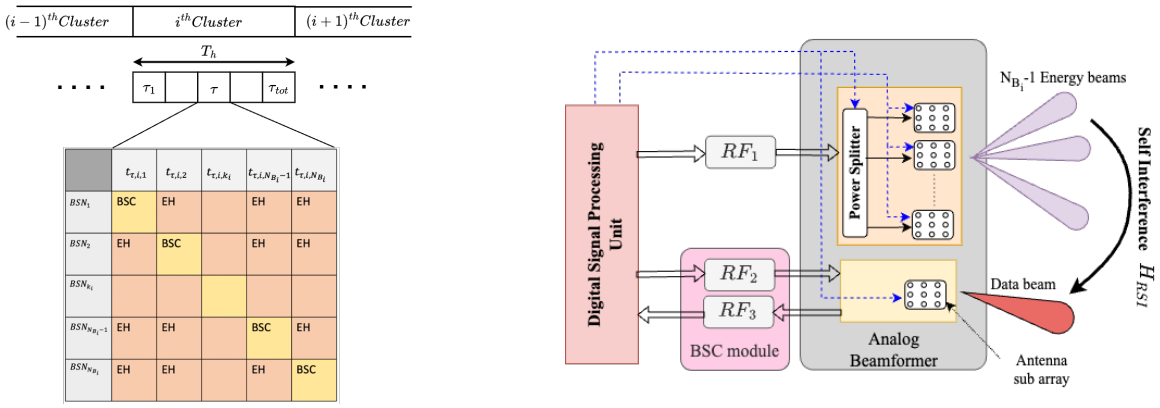

(a) (b)

Figure 2: (a) Proposed multi-BSN serving protocol: Illustrating the total hovering time T_h for the i^{th} cluster with N_{B_i} BSNs, partitioned into τ_{tot} intervals, each interval further segmented into N_{B_i} slots. (b) Proposed transceiver architecture at the UAV.

to a single separate sub-array of size $N_x \times N_y$, which generates a steerable BSC beam towards the BSN for its data collection. RF_2 transmits an unmodulated amplified carrier signal, while RF_3 serves as the BSC receiver to receive the modulated signal reflected by the BSN. Thus, the proposed joint WET and BSC transceiver architecture at the UAV with only three RF chains reduces UAV hardware cost as well as power consumption.

C. Channel Model

Let, $d_{v,k}=\|X_v - X_k\|$ denote the Euclidean distance between the UAV and the k^{th} BSN, and ϕ_k, θ_k be the azimuth angle and elevation angle, respectively, of k^{th} BSN. The UAV-to-BSN channel is considered line-of-sight (LoS) dominant [5] due to the low altitude of the UAV and highly directional mmWave beam it uses. Thus, the path loss experienced by k^{th} BSN is [22]

$$\text{PL}_k=10^{-\left(a+\mu 10\log_{10}\left(d_{u,k}\right)+n\right)/10}. \tag{1}$$

Here, a, μ, and, $n \sim \mathcal{N}(0,\sigma_s^2)$ respectively denote frequency-dependent constant, path loss exponent, and log-normal shadowing loss factor . The transmit array response vector $\mathbf{a}(\phi,\theta) \in \mathbb{C}^{1\times N_x N_y}$ of a sub-array of size $N_x \times N_y$ at an azimuth angle ϕ and elevation angle θ is expressed as

$$\mathbf{a}(\phi,\theta)=\frac{1}{N_x N_y}\left[1,\cdots,e^{-j\frac{2\pi}{\lambda}\tilde{d}\sin\theta[(N_x-1)\cos\phi+(N_y-1)\sin\phi]}\right]^T. \tag{2}$$

Here, $\tilde{d}$ is the inter antenna element spacing and λ is the wavelength. Therefore, the channel between k^{th} BSN and the UAV is given by

$$\mathbf{h}_k = \sqrt{N_x N_y G_0 \text{PL}_k}\,\alpha_k \mathbf{a}_T^H(\phi_k, \theta_k) \in \mathbb{C}^{1\times N_x N_y}. \tag{3}$$

Here, α_k denotes the complex channel fading gain modeled using Rician distribution, parameterized by Rician factor K_r, and G_0 is per antenna element gain. Moreover, we assume block fading model and complete CSI availability at the UAV transceiver obtained via standard channel estimation procedures [23]. The steering direction $\{\tilde{\phi}, \tilde{\theta}\}$ of the beams are controlled by phase shifters, which generates discrete phase shift controlled by control registers of size b_s bits. Let, Φ and Θ denote the set of possible azimuthal and elevation steering directions, respectively, such that

$$\Phi = \left\{ \frac{2\pi i}{2^{b_s}} | i = 0, 1, \cdots, 2^{b_s} - 1 \right\},\ \Theta = \left\{ \frac{2\pi j}{2^{b_s+1}} | j = 0, 1, \cdots, 2^{b_s} - 1 \right\}.$$

Due to finite resolution, the beam cannot be steered exactly toward the BSN. Therefore, the optimal steering direction for the k^{th} BSN $\forall k \in \{1, 2, \cdots, N_{Bi}\}$ is given by

$$\tilde{\phi}_k = \arg\min_{\tilde{\phi}_i \in \Phi} |\phi_k - \tilde{\phi}_i|,\ \tilde{\theta}_k = \arg\min_{\tilde{\theta}_j \in \Theta} |\theta_k - \tilde{\theta}_j|.$$

Let, $\mathbf{A}_{RF} \in \mathbb{C}^{N_B \times N_x N_y}$ be the analog precoding matrix of the sub-array hybrid structure such that $\mathbf{A}_{RF} = \{\mathbf{a}_1, \cdots, \mathbf{a}_k, \cdots, \mathbf{a}_{N_B}\}$, where $\mathbf{a}_k$ is the RF steering vector for steering the beam towards k^{th} BSN governed by $\{\tilde{\phi}_k, \tilde{\theta}_k\}$. It is expressed as

$$\mathbf{a}_k = \left[1, \cdots, e^{-j(2\pi/\lambda)\tilde{d} \sin\tilde{\theta}_k [(m-1)\cos\tilde{\phi}_k + (n-1)\sin\tilde{\phi}_k]} \right] \forall m, n \in \mathbb{Z}; (k-1)\sqrt{N_x N_y} + 1 \le m, n \le k\sqrt{N_x N_y}. \tag{4}$$

D. Modeling of RSI at UPA

In a full-duplex transceiver, perfect self-interference cancellation is not possible [24], [25]. We model the RSI channel matrix $\mathbf{H}_{j,k}^{\text{RSI}}$ between the j^{th} transmitter array of size $N_{x_t} \times N_{y_t}$ and k^{th} receiver array of size $N_{x_r} \times N_{y_r}$ as $\mathbf{H}_{j,k}^{\text{RSI}} = \mathbf{H}_{LoS} + \mathbf{H}_{NLoS} \in C^{N_{x_t} N_{x_r} \times N_{y_t} N_{y_r}}$, where $\boldsymbol{H}_{LoS}$ and $\mathbf{H}_{NLoS}$ denote LoS and NLoS components, respectively. Let, $\{i, p\} \in \mathbb{Z}^+$ and $\{j, q\} \in \mathbb{Z}^+$ denote the index of antenna elements along the x-axis and y-axis of transmit and receive subarrays, where $0 \le i < N_{t_x}$, $0 \le j < N_{t_y}$, $0 \le p < N_{r_x}$, and $0 \le q < N_{r_y}$. Then the LoS and NLoS

components of RSI channel between the $(i, j)^{\text{th}}$ transmit antenna and $(p, q)^{\text{th}}$ receiver antenna element pair, as modeled in [26], are

$$\mathbf{H}_{LoS}(i \cdot p, j \cdot q) = \frac{\kappa}{\Delta_{(i,j)-(p,q)}} e^{-j2\pi\Delta_{(i,j)-(p,q)}}, \tag{5}$$

$$\text{and, } \mathbf{H}_{NLoS}(i \cdot p, j \cdot q) \sim \mathcal{N}(0, \sigma^2_{NLoS}). \tag{6}$$

Here, $\Delta_{(i,j)-(p,q)} = \sqrt{\left[D_y^2 + ((j-q)\tilde{d})^2\right] + \left[(i-1)\tilde{d} + (p-1)\tilde{d} + D_x\right]^2}$ is the distance between the antenna element pair normalized by the wavelength, κ denotes the normalization scalar depending on the achievable self-interference cancellation, D_x and D_y respectively denote the antenna array separation distances along x-axis and y-axis normalized by wavelength.

E. Modeling of UAV Power Consumption

To serve N BSNs, the UAV performs two broad operations: communication and maneuvering. Thus, UAV power consumption comprises of consumptions in the communication module and in UAV maneuvering operations.

Power consumption in the communication module is composed of two main components: transmission and consumption in communication hardware. Transmit power denotes the overall power transmitted by the UAV to facilitate energy harvesting and data offloading operations. Each transmitter RF front end comprises a pair of digital-to-analog converters, a mixer, a low pass filter, a local oscillator, and a power amplifier connected to the antenna subarray. On the other hand, the receiver RF front end consists of a low noise amplifier attached to each antenna element of the subarray, an analog-to-digital converter pair, a low pass filter, and a mixer. We assume negligible power consumption in phase shifters and power splitters. Accordingly, the total hardware power consumption of the proposed transceiver is obtained as

$$P_c = 2 \times 2\,(P_{\text{DAC}} + P_{\text{M}} + P_{\text{LPF}}) + P_{tot}/\eta_{\text{PA}} + P_{\text{O}} + P_{\text{LNA}} N_{\text{t}} + 2P_{\text{ADC}} + P_{\text{LPF}} + P_{\text{M}}. \tag{7}$$

Therefore, for a given UAV communication power budget P_{com}, the power available for transmission purposes is $P_{tot} = P_{com} - P_c$.

UAV maneuvering power consumption comprises of two main components: hovering and movement. The power required for UAV movement $P_{mov}(V)$ is given by [27]

$$P_{mov}(V) = P_o \left(1 + \frac{3V^2}{U_{tip}^2}\right) + \frac{P_i v_o}{V} + \frac{1}{2} d_o \rho s A V^3, \tag{8}$$

where $P_o{=}\delta\rho s A\Omega^3 R^3/8$ and $P_i{=}(1+k_e)W^{3/2}/\sqrt{2\rho A}$. Further, the power consumed in hovering is $P_{hov}{=}P_o+P_i$. Description of various constants used in (7) and (8) are summarized in Table I.

F. Received Signal and Harvested Energy

For a given total transmission power P_{tot}, let, $|b_{\tau,i,k}|^2$ be the power allocated to k^{th} BSN, where $b_{\tau,i,k} \in \mathbb{R}^+$ and $k{=}\{1,\ldots,N_{Bi}\}$, served by a beam (either energy beam or data beam) during τ^{th} interval over i^{th} cluster such that $\sum_{j=1}^{N_{Bi}} |b_{\tau,i,j}|^2 \leq P_{tot}\ \forall i$. Then, the downlink signal received at the k^{th} BSN of i^{th} cluster is

$$\hat{y}_{\tau,i,k}{=}(\mathbf{h}^D_{\tau,i,k})^H \mathbf{a}_{i,k} b_{\tau,i,k} s_{\tau,i,k} + z^D_{\tau,i,k}. \tag{9}$$

Here, $\mathbf{h}^D_{\tau,i,k}$ is the downlink channel (of the form given by (3)), $z^D_{\tau,i,k}$ is the downlink additive white Gaussian noise, $\mathbf{a}_{i,k}$ is the RF steering vector (by (4)), and $s_{\tau,i,k}$ is unit power transmitted signal to k^{th} BSN of the cluster. Within slot $t_{\tau,i,k}$, the k^{th} BSN modulates $\hat{y}_{\tau,i,k}$ according to its data and reflects it back towards the UAV in the same direction that is processed by BSC receiver at RF_3. Therefore, BSN modulated signal received by the UAV in its uplink is

$$y_{\tau,i,k}{=}\underbrace{\sqrt{1-\beta_{\tau,i,k}}\mathbf{a}^H_{i,k}\mathbf{h}^U_{\tau,i,k}(\mathbf{h}^D_{\tau,i,k})^H\mathbf{a}_{i,k}b_{\tau,i,k}s_{\tau,i,k}x_{\tau,i,k}}_{\text{Desired component}} + \underbrace{\mathbf{a}^H_{i,k}\mathbf{h}^U_{\tau,i,k}z^D_{\tau,i,k}+z^U_{\tau,i,k}}_{\text{Noise component}} + \underbrace{\sum_{j\neq k}\mathbf{a}^H_{i,k}\mathbf{H}^{\text{RSI}}_{\tau,j,k}\mathbf{a}_{i,j}b_{\tau,i,j}s_{\tau,i,j}}_{\text{RSI component}}. \tag{10}$$

Here, $\mathbf{h}^U_{\tau,i,k}$ is the uplink channel of the form given by (3), $\beta_{\tau,i,k} \in \mathbb{R}$ is the reflection coefficient, $x_{\tau,i,k}$ is the superimposed information signal, and $z^U_{\tau,i,k}$ is the uplink Gaussian noise for k^{th} BSN. Consequently, the data rate of k^{th} BSN over the time $t_{\tau,i,k}$ is

$$r_{\tau,i,k}{=}\log_2\left(1+\frac{\left|\mathbf{a}^H_{i,k}\mathbf{h}^U_{\tau,i,k}(\mathbf{h}^D_{\tau,i,k})^H\mathbf{a}_{i,k}b_{\tau,i,k}\right|^2(1-\beta_{\tau,i,k})}{\sum_{j\neq k}\left|\mathbf{a}^H_{i,k}\mathbf{H}^{\text{RSI}}_{\tau,j,k}\mathbf{a}_{i,j}b_{\tau,i,j}\right|^2+\sigma^2\left(\left|\mathbf{a}^h_{i,k}\mathbf{h}^U_{\tau,i,k}\right|^2+1\right)}\right). \tag{11}$$

It is notable here that the power allocated by the UAV to a BSN remains constant during the entire τ^{th} interval consisting of N_{Bi} time slots. This means that the UAV sends the same power to the set of BSNs throughout the τ^{th} interval. Let, $P^{in}_{t_{\tau,i,j},k}$ denote the input power at the front end of the energy harvesting module of k^{th} BSN during $t_{\tau,i,j}$ time slot where j and $k \in \{1,\cdots,N_{Bi}\}$.

Then, the power harvested by a BSN considering a non-linear energy harvesting model [28]–[30] is

$$\eta\left(P^{in}_{t_{\tau,i,j},k}\right)=\frac{\frac{P_0}{1+\exp(-\upsilon(P^{in}_{t_{\tau,i,j},k}-\vartheta))}-\frac{P_0}{1+\exp(\upsilon\vartheta)}}{1-\frac{1}{1+\exp(\upsilon\vartheta)}}. \tag{12}$$

Here, P_0 denotes the maximum possible harvest power, and $\{\upsilon,\vartheta\}$ denotes the shaping parameters. Importantly, $\eta\left(P^{in}_{t_{\tau,i,j}k}\right)$ is neither concave nor convex with respect to $|b_{\tau,i,k}|^2$. However $\eta\left(P^{in}_{t_{\tau,i,j}k}\right)$ is a monotonically increasing and injective function with respect to $|b_{\tau,i,k}|^2$ [31]. Let, $\Psi(\eta)$ be the inverse function of $\eta\left(P^{in}_{t_{\tau,i,j}k}\right)$, which is expressed as [29, Eq. (22)]

$$\Psi(\eta)=\vartheta-\frac{1}{\upsilon}\ln\frac{e^{\upsilon\vartheta}(P_0-\eta)}{e^{\upsilon\vartheta}\eta+P_0}. \tag{13}$$

It may be further noted here that, during the WET phase, the power received by the energy harvestor module of the k^{th} BSN is utilized for energy harvesting. Mathematically, this is expressed as $P^{in}_{t_{\tau,i,j},k}=\left|\hat{y}_{\tau,i,k}\right|^2\ \forall j\neq k$. In contrast, during the data collection phase ($j=k$), a portion of the received power is allocated for energy harvesting, which depends on the reflection coefficient $\beta_{\tau,i,k}$ of the k^{th} BSN, i.e., $P^{in}_{t_{\tau,i,j},k}=\beta_{\tau,i,k}\left|\hat{y}_{\tau,i,k}\right|^2$, while the remaining power is utilized for transmitting data at an achievable rate, as given by (12).

III. Problem Formulation and Optimization

In the proposed system model for UAV-aided BSC based data collection and wireless charging of BSNs, as described in Section II, we aim to maximize the sum of data collected (weighted by ς_1) and energy harvested (weighted by ς_2) by the BSNs deployed in the region of interest.

A. Optimization Problem Formulation

Let, $\mathcal{G}_{i,\tau}(\mathbf{t},\boldsymbol{\beta},\mathbf{b},\mathbf{u})=\sum_{k=1}^{N_{Bi}}\varsigma_1 D_{\tau,i,k}+\varsigma_2 E_{\tau,i,k}$ denote the joint objective function for the i^{th} cluster in the τ^{th} time interval. Here, $D_{\tau,i,k}=t_{\tau,i,k}r_{\tau,i,k}$ and $E_{\tau,i,k}=\sum_{j=1}^{N_{Bi}}t_{\tau,i,j}\eta(P^{in}_{t_{\tau,i,j},k})$ denote the data collected and energy harvested, respectively, by k^{th} BSN of i^{th} cluster. Therefore, the optimizing variables for i^{th} cluster are: vector of UAV's transmit power coefficients $\mathbf{b}$, vector of data offloading time $\mathbf{t}$, and vector of BSN reflection coefficients $\boldsymbol{\beta}$. ς_1 and ς_2 are the scaling weights and the ratio ς_2/ς_1 specifies the degree to which maximizing energy harvesting takes precedence over data offloading. Additionally, we optimize the number of BSN clusters N_c. Therefore, the overall problem formulation is defined as

$$
\begin{aligned}
(\mathcal{P}1): \quad & \max_{N_c,\{\mathbf{t},\boldsymbol{\beta},\mathbf{b}\}\forall i,\tau} \quad \sum_{i=1}^{N_c}\sum_{\tau=1}^{T_{tot}}\sum_{k=1}^{N_{Bi}} \varsigma_1 D_{\tau,i,k} + \varsigma_2 E_{\tau,i,k} \\
\text{s.t.}: \quad & (C_1): \sum_{k=1}^{N_{Bi}} |b_{\tau,i,k}|^2 \leq P_{tot} && \forall i,\tau \\
& (C_2): E_{\tau,i,k} \geq t_{\tau,i,k} P_{\text{BSN}} + E_{\text{th}} && \forall k,\tau,i \\
& (C_3): t_{\tau,i,k} r_{\tau,i,k} \geq D_{\text{th}} && \forall k,\tau,i \\
& (C_4): \sum_{k=1}^{N_{Bi}} t_{\tau,i,k} \leq 1 && \forall i,\tau \\
& (C_5): 0 \leq \beta_{\tau,i,k} \leq 1 && \forall k,\tau,i \\
& (C_6): 0 \leq t_{\tau,i,k} \leq 1 && \forall k,\tau,i \\
& (C_7): \sum_{k=1}^{N_{Bi}} \delta_{i,k} \leq N_B^{max} && \forall i \\
& (C_8): R_i \leq R_{max} && \forall i \\
& (C_9): \sum_{i=1}^{N_c} \delta_{i,k} \leq 1 && \forall k \\
& (C_{10}): N_c \in \mathbb{Z}^+.
\end{aligned}
\tag{14}
$$

The constraint (C_1) ensures that the total transmission power allocated to every cluster is less than or equal to the communication power budget of the UAV. (C_2) and (C_3) ensure that the data offloaded and the energy harvested by each BSN meet their respective minimum requirements. (C_4) indicates that the duration of each interval is normalized to unity. (C_5) and (C_6) bound the values of the backscatter reflection coefficient and data offloading time for all BSNs. (C_7) limits the maximum number of BSNs that can be accommodated in a cluster and served simultaneously which is governed by the maximum number of antenna sub arrays N_B^{max} at the UAV. (C_8) imposes an upper bound on the cluster radius R_i. (C_9) highlights that a BSN can be associated with only one cluster, where the BSN cluster association indicator variable $\delta_{i,k}$ is defined as

$$
\delta_{i,k} = \begin{cases} 1 & k^{\text{th}} \text{ BSN lies in } i^{\text{th}} \text{ cluster} \\ 0 & \text{otherwise.} \end{cases}
\tag{15}
$$

Additionally, different notations used in $(\mathcal{P}1)$ are summarized in Table I. The problem $(\mathcal{P}1)$ is multivariate, and the variables are closely coupled in objective function and constraints. Thus,

making it non-convex and non-deterministic polynomial-time hard (NP-hard). Therefore, we solve it using a sub-optimal approach, as discussed next.

B. Optimization of BSN Clustering and Visiting Sequence

To optimize resource allocation per cluster in ($\mathcal{P}1$), we first optimize the number of clusters N_c that depends on the adopted BSNs clustering strategy. Generally, a small value of N_c with large cluster dimensions is desired to serve more BSNs per cluster during T_h. However, there exist restrictions on both parameters. Let, θ_s^{max} be a UPA's maximum possible elevation steering angle. Then, the maximum allowable cluster radius is R_{max}=$h_{\text{UAV}} \tan\left(\theta_s^{max}\right)$. Besides R_{max}, the value of N_c depends on the number of beams N_B generated at the UAV as well. Increasing N_B allows to serve more BSNs simultaneously and collect more data simultaneously. However, there is a trade-off because more beams also increase RSI, which can negatively affect data collection. Therefore, we estimate optimal number of beams N_B^* a priori in offline mode with the proposed transceiver design while still satisfying the minimum requirements for data collection and energy charging to all BSNs of a cluster. Subsequently, this estimated value is utilized during the optimal clustering of BSNs.

1) Estimation of N_B^*: Employing the proposed UAV transceiver architecture, BSN receives dedicated communication through an individual beam. This means that with N_B beams, maximum N_B number of BSNs can be accommodated within a cluster of radius R_{max}. For offline N_B^* estimation process, we assume that the channel coherence time is divided into N_B equal slots, i.e., t_j=t_c/N_B for all j. Additionally, for mathematical simplicity, we consider that the reflection coefficients of all BSNs are fixed.

Increasing the value of N_B allows to serve more BSNs within a cluster. However, as N_B increases, the total communication power required by the UAV to fulfill the minimum data collection and energy harvesting requirements also increases. Consequently, the minimum communication energy used by the UAV during a channel coherence time interval is given as

$$E_{tot}=\sum_{k=1}^{N_B}\sum_{j=1}^{N_B} P_{j,k}t_j. \tag{16}$$

Here, $P_{j,k}$ is the transmission power at k^{th} BSN in j^{th} slot. Also, the total minimum data collected is D_{tot}=$N_B D_{\text{th}}$. For offline estimation of N_B^*, we maximize the total energy efficiency

(EE), which is defined as the ratio of total data collected by the UAV to the total energy spent by it, i.e.,

$$\mathrm{EE}(N_B)=\frac{D_{tot}}{E_{tot}}=\frac{N_B D_{\mathrm{th}}}{\sum_{k=1}^{N_B}\sum_{j=1}^{N_B} P_{j,k}t_j}. \tag{17}$$

In each slot, the transmit power of each beam is determined to fulfill the minimum data rate and energy requirement. The overall procedure to estimate N_B^* that maximizes $\mathrm{EE}(N_B)$ while meeting the minimum energy transfer E_{th} and minimum data collection D_{th} constraints of all BSNs in a cluster is given in Algorithm 1, and the steps are as follows:

(i) Initially assuming zero RSI, calculate the power required for minimum data collection for each BSN.

(ii) Calculate transmit power of all energy beams in all slots such that

$$\sum_{j,j\neq k} t_j \eta(P_{j,k}) = t_j P_{\mathrm{BSN}} + E_{\mathrm{th}} \ \forall k, \tag{18}$$

where $\{P_{j,k}\}$ solved using (18) ensures that each BSN harvests sufficient energy in (N_B-1) slots to transmit at least D_{th} data bits and harvest additional energy.

(iii) Due to $\{P_{j,k}\}$, each BSN sees some RSI that reduces the effective data collection rate $r_k < D_{\mathrm{th}}/t_k$ of each BSN. Update the RSI component using (10) and recalculate the transmission power for collecting D_{th} data bits from each BSN, considering the RSI into account.

(iv) Calculate $\mathrm{EE}(N_B)$ using (17).

(v) Increment the value of N_B and repeat steps (i)-(iv).

(vi) Finally $N_B^* = \underset{N_B}{argmax}\ \mathrm{EE}(N_B)$.

2) Determination of BSN Clustering and Cluster Visiting Sequence: We now solve for the minimum possible value of N_c for a given maximum cluster radius R_{max} and the corresponding optimization problem is

$$\begin{aligned} (\mathcal{P}2): \ & \min_{\{\delta_{i,k}\}} \ N_c \\ & \text{s.t.}: \ (C_7), (C_8), (C_9), (C_{10}). \end{aligned} \tag{19}$$

$(\mathcal{P}2)$ is solved using a modified version of the artificial bee colony (ABC) based algorithm presented in [12]. The algorithm comprises multiple iterations, where in n^{th} iteration, the set of BSNs associated with n^{th} cluster is determined. In the first step, the boundary set of the unclustered BSNs location is obtained by the convex hull algorithm. Based on that, the location

Algorithm 1 Algorithm to estimate N_B^*

Input: CSI, D_{th}, E_{th}, $\mathcal{X}_u$, $\mathcal{X}_v$
Output: N_B^*
for N_B=N_B^{min} to N_B^{max} **do**
    Set RSI component zero $\forall k$
    for k=1 to N_B **do**
        Calculate $\{P_{k,k}\}_{\forall k}$ such r_k=D_{th}/t
    end for
    for k=1 to N_B **do**
        Calculate $P_{j,k_{\forall j \neq k}}$ using (18)
    end for
    Update RSI components using (10)
    for k=1 to N_B **do**
        Calculate $\{P_{k,k}\}_{\forall k}$ such r_k=D_{th}/t
    end for
    Calculate EE(N_B) using (17)
end for
N_B^*=$\underset{N_B}{argmin}$EE(N_B)

set is partitioned into a boundary set and an inner point set. Thereafter, the farthest located BSN from the centroid of the unclustered BSN is picked. We called it the root BSN around which the n^{th} cluster is formed. The neighborhood points across the root BSN within the distance of $2R_{max}$ are taken into consideration. This is done to reduce the search space. After that, by using the ABC algorithm, the cluster centroid is obtained, and the BSNs located within the neighborhood of the centroid (within a radius denoted as R_{max}) are grouped together into a cluster.

The ABC algorithm is an iterative three-phase algorithm. Initially a set of potential centroid locations are generated around the root BSN. In the first phase, i.e., the employed phase, all the candidate locations are updated with newly generated random locations via a greedy approach. Based on their fitness value, the best location is chosen as a centroid. In contrast to the linear fitness function used in [12], we employ a truncated discrete Gaussian shape-based fitness function. This fitness function assigns the highest weight to clusters that contain precisely N_B^* BSNs. We denote this clustering method as mABC. Therefore, the proposed mABC clustering algorithm prioritizes clusters where N_{Bi}, matches N_B^*. It is important to note that with the mABC

clustering, some clusters will have $N_{Bi} \neq N_B^*$, as N_{Bi} can range up to N_B^{max}. In the second phase, i.e., the onlooker phase, the candidate locations are chosen probabilistically and are updated based on the fitness value. Afterward, the candidate locations having fitness value that has not improved over a predefined number of sub-iterations are abandoned from the further searching process. In the last scout phase, the abandoned candidate locations are clubbed together and replaced by new random locations. These three phases are repeated until convergence is achieved. Once the n^{th} cluster centroid and the associated BSN index are found, they are eliminated from the search set. A similar process is repeated in the next iterations until all the BSNs are clustered.

Subsequently, the sequence of clusters the UAV needs to visit ($\mathcal{V}_s$) is determined using a traveling salesman problem (TSP) based approach. By employing the TSP methodology [32], the problem is transformed into a graph computational problem in which the UAV needs to find the route with the minimum maneuvering power consumption to visit all the cluster centroids exactly once and return to the starting point. The locations of the cluster centroids are obtained from ($\mathcal{P}2$). Then, the distances between each pair of centroids are calculated, and the power consumption associated with maneuvering between each pair using equation (8) is evaluated and stored in a lookup table. An initial path/graph is generated such that the UAV begins from the initial position and chooses the nearest unvisited cluster. This process is continued until all the clusters have been visited. Thereafter, pairwise swapping is carried out, and its impact on power consumption is evaluated. If the resultant path consumes relatively less energy, then the swap is executed. The continual assessment and potential swapping are carried out iteratively until no further improvement can be made. This approach allows to determine the least number of clusters and the shortest route to cover their centroids.

C. Alternating Optimization for Resource Allocation

In addition, during the service of a specific cluster, we aim to optimize the parameters $\mathbf{b}$, $\mathbf{t}$, and $\boldsymbol{\beta}$ $\forall i, \tau$, while satisfying the minimum energy transfer and data collection constraints within the communication energy budget of the UAV.

It is to be noted that the resrouce allocation is carried out independently for every time interval. To simplify the notation, we will omit the subscript i and τ in the subsequent discussion. Since the $\eta(P_{in})$ is an increasing function with respect to b_k therefore using [33, Lemma 2] we simplify the objective function by substituting $\varsigma_2 E_k$ by $\varsigma_2 \mathcal{E}_k$ where $\mathcal{E}_k = b_k |(\mathbf{h}_k^D)^H \mathbf{a}_k|^2 \left(t_k \beta_k + \sum_{j=1, j\neq k}^{N_B} t_j \right)$.

Therefore, the optimization of joint resource allocation for the i^{th} cluster consisting of N_{Bi} BSNs during τ^{th} interval is formulated as

$$\begin{aligned}(\mathcal{P}3): \quad & \max_{\mathbf{b},\boldsymbol{\beta},\mathbf{t}} \quad \sum_{k} \varsigma_1 t_k r_k + \varsigma_2 \mathcal{E}_k \\ & \text{s.t.}: \quad (C_1), (C_2), (C_3), (C_4), (C_5), (C_6).\end{aligned} \tag{20}$$

The problem $(\mathcal{P}3)$ is a non-convex NP-hard problem, and therefore we solve it using an alternating optimization approach. In each iteration, one subset of variables is optimized while the other variables are fixed, and then the roles of the subsets are switched in the next step. This iterative process continues until a stopping criterion is met.

1) BSN power allocation: Here, an iterative algorithm to design $\mathbf{b}$ is presented. Fixing $\boldsymbol{\beta}$ and $\mathbf{t}$, the optimal value $\mathbf{b}^*$ can be obtained by solving the following optimization problem.

$$\begin{aligned}(\mathcal{P}4): \quad & \max_{\mathbf{b}} \quad \sum_{k} \varsigma_1 t_k r_k + \varsigma_2 \mathcal{E}_k \\ & \text{s.t.}: \quad (C_1), (C_2), (C_3).\end{aligned} \tag{21}$$

The objective function and constraint (C_3) in the power allocation problem $(\mathcal{P}4)$ are inherently non-concave due to the interplay between transmitted signals and the related RSI.

To solve the problem, auxiliary variables $\boldsymbol{\varrho}$ and $\boldsymbol{\zeta}$ are introduced where the former represents SNR and the latter represents noise and interference power at the receiver side of the UAV. Thereafter sequential convex approximation method is applied which successively relaxes the original non-convex problem, transforming it into a series of convex subproblems. Over the iterations the solution is refined, leading to an increasingly improved power allocation vector and thus a suboptimal power allocation vector is obtained.

Using $\boldsymbol{\varrho}$, the objective function in $(\mathcal{P}4)$ can be transformed to a concave form and is represented as $\mathcal{F}(\boldsymbol{\varrho}, \boldsymbol{\zeta}, \mathbf{b}) = \sum_k \varsigma_1 t_k \log(1+\varrho_k) + \varsigma_2 \mathcal{E}_k$. Further using (13), constraint (C_2) is simplified as $(\hat{C_2}): b_k > ((1/|(\mathbf{h}_k^D)^H \mathbf{a}_k|^2)\Psi((t_k P_{\text{BSN}} + E_{th})/1-t_k))^{1/2}$. Therefore an equivalent optimization problem is expressed as

$$\begin{aligned}(\mathcal{P}4.1): \quad & \max_{\boldsymbol{\varrho},\boldsymbol{\zeta},\mathbf{b}} \quad \mathcal{F}(\boldsymbol{\varrho}, \boldsymbol{\zeta}, \mathbf{b}) \\ & \text{s.t.}: \quad (C_1), (\hat{C_2}) \\ & \qquad (\hat{C_3}): \zeta_k \geq 2^{D_{th}/t_k - 1} \\ & \qquad (\hat{C_4}): \left| \sqrt{(1-\beta_k)} \mathbf{a}_k^H \mathbf{h}_k^U (\mathbf{h}_k^D)^H \mathbf{a}_k \right| b_k \geq \sqrt{\zeta_k \varrho_k} \\ & \qquad (\hat{C_5}): \sum_{j \neq k} \left| \mathbf{a}_k^H \mathbf{H}_{j,k}^{\text{RSI}} \mathbf{a}_j \right|^2 b_j^2 + \sigma^2 \left(\left| \mathbf{a}_k^h \mathbf{h}_k^U \right|^2 + 1 \right) \leq \zeta_k.\end{aligned} \tag{22}$$

In (22), constraint $(\hat{C}3)$ imposes concave lower bound on the received SNR. $(\hat{C}4)$ and $(\hat{C}5)$ establishes the relationship between the auxiliary variables and the data rate. The constraints $(\hat{C}3)$ and $(\hat{C}5)$ are convex however $(\hat{C}4)$ is non-convex due to square root term. Using first order Taylor series expansion we have $\sqrt{\zeta_k, \varrho_k} \leq G(\zeta_k, \varrho_k)$ where

$$G(\zeta_k^{(\ell)}, \varrho_k^{(\ell)})=\sqrt{\zeta_k^{(\ell-1)}\varrho_k^{(\ell-1)}} \;+\; \frac{1}{2}\sqrt{\frac{\zeta_k^{(\ell-1)}}{\varrho_k^{(\ell-1)}}}\left(\varrho_k^{(\ell)} - \varrho_k^{(\ell-1)}\right) \;+\; \frac{1}{2}\sqrt{\frac{\varrho_k^{(\ell-1)}}{\zeta_k^{(\ell-1)}}}\left(\zeta_k^{(\ell)} - \zeta_k^{(\ell-1)}\right) \quad (23)$$

and $\zeta_k^{(\ell-1)}, \varrho_k^{(\ell-1)}$ represents the optimizing parameters after $(\ell-1)^{\text{th}}$ iteration. Using the above approximation, (22) is transformed into a convex optimization problem, expressed as

$$\begin{aligned}(\mathcal{P}4.2): \quad &\max_{\boldsymbol{\varrho},\boldsymbol{\zeta},\mathbf{b}} \quad \mathcal{F}(\boldsymbol{\varrho}, \boldsymbol{\zeta}, \mathbf{b}) \\ &\text{s.t.}: \quad (C_1), (\hat{C}_2), (\hat{C}_3), (\hat{C}_5) \\ &\qquad (\hat{C}_4): \left|\sqrt{(1-\beta_k)}\mathbf{a}_k^H \mathbf{h}_k^U (\mathbf{h}_k^D)^H \mathbf{a}_k\right| b_k \geq G(\zeta_k, \varrho_k).\end{aligned} \quad (24)$$

The procedure to obtain $\mathbf{b}^*$ via SCA method is summarized in Algorithm 2.

Algorithm 2 SCA method based algorithm to solve $(\mathcal{P}4)$

1: Input : CSI, D_{th}, E_{th}, $\mathcal{X}_u$, $\mathcal{X}_v$, $|N_B|$, $\boldsymbol{\beta}^*$, $\mathbf{t}^*$
2: Initialize : $\mathbf{b}^0, \boldsymbol{\zeta}^0, \boldsymbol{\varrho}^0, \ell$=0
3: Output : $\mathbf{b}^*$
4: **do**
5: Update $\mathcal{F}_{old} \leftarrow \mathcal{F}(\mathbf{b}^{(\ell)}, \boldsymbol{\zeta}^{(\ell)}, \boldsymbol{\varrho}^{(\ell)})$
6: Update $\ell \leftarrow \ell + 1$
7: Obtain $(\mathbf{b}^{(\ell)}, \boldsymbol{\zeta}^{(\ell)}, \boldsymbol{\varrho}^{(\ell)})$ by solving $(\mathcal{P}4.2)$.
8: Update $\mathbf{b}^* \leftarrow \mathbf{b}^{(\ell)}$
9: **while** $\left|\mathcal{F}(\mathbf{b}^{(\ell)}, \boldsymbol{\zeta}^{(\ell)}, \boldsymbol{\varrho}^{(\ell)}) - \mathcal{F}_{old}\right| \geq \epsilon_o$ or $\ell \leq \ell_{max}$

2) Reflection coefficient optimization: Given that $\mathbf{b}^*$ and $\mathbf{t}^*$ are known, optimal value $\boldsymbol{\beta}^*$ can be evaluated by solving the following optimization problem

$$\begin{aligned}(\mathcal{P}5): \quad &\max_{\boldsymbol{\beta}} \quad \sum_k \varsigma_1 t_k r_k + \varsigma_2 \mathcal{E}_k \\ &\text{s.t.}: \quad (C_2), (C_3), (C_5).\end{aligned} \quad (25)$$

In ($\mathcal{P}5$), the objective function is concave. Further simplifying the constraint (C_2) using (13), ($\mathcal{P}5$) is redefined as

$$\begin{aligned}(\mathcal{P}5.1): \quad & \max_{\boldsymbol{\beta}} \quad \sum_k \varsigma_1 t_k r_k + \varsigma_2 \mathcal{E}_k \\ & \text{s.t.}: \quad (\tilde{C_2}): \beta_k > (1/|\hat{y}_k|^2) \times \Psi((t_k P_{\text{BSN}} + E_{th} - (1-t_k)\eta(|\hat{y}_k|^2))/t_k) \forall k, \\ & \qquad\quad (C_3), (C_5).\end{aligned} \tag{26}$$

The overall problem ($\mathcal{P}5.1$) is convex and can be solved by any standard convex optimization technique.

3) Communication time optimization: Given $\mathbf{b}^*$ and $\boldsymbol{\beta}^*$, optimal value $\mathbf{t}^*$ is obtained by solving the following problem

$$\begin{aligned}(\mathcal{P}6): \quad & \max_{\mathbf{t}} \quad \sum_k \varsigma_1 t_k r_k + \varsigma_2 E_k \\ & \text{s.t.}: \quad (C_2), (C_3), (C_4), (C_6).\end{aligned} \tag{27}$$

In the above problem, the objective function and all the constraints are linear function in terms of the optimization variable. Therefore, the problem ($\mathcal{P}6$) is a linear optimization problem and can be solved by the interior point method.

The alternating optimization procedure used to solve problem ($\mathcal{P}3$) is outlined in Algorithm 3. It involves breaking down the original problem ($\mathcal{P}3$) into three subproblems, namely ($\mathcal{P}4$), ($\mathcal{P}5$), and ($\mathcal{P}6$). The algorithm iteratively optimizes each set of variables while keeping the others fixed. This iterative process continues until convergence is achieved or a maximum number of iterations is reached.

Algorithm 3 Algorithm to solve ($\mathcal{P}3$)

1: Input : CSI, D_{th}, E_{th}, $\mathcal{X}_u$, $\mathcal{X}_v$, q=1
2: Output : $\mathbf{b}^*, \boldsymbol{\beta}^*, \mathbf{t}^*$
3: **do**
4: $\quad q \leftarrow q + 1$
5: $\quad$ Given $\mathbf{t}^{(q)}$ and $\boldsymbol{\beta}^{(q)}$, find $\mathbf{b}^{(q+1)}$ by solving ($\mathcal{P}4$)
6: $\quad$ Given $\mathbf{t}^{(q)}$ and $\mathbf{b}^{(q+1)}$, find $\boldsymbol{\beta}^{(q+1)}$ by solving ($\mathcal{P}5$)
7: $\quad$ Given $\boldsymbol{\beta}^{(q+1)}$ and $\mathbf{b}^{(q+1)}$, find $\mathbf{t}^{(q+1)}$, by solving ($\mathcal{P}6$)
8: **while** $\left|\mathcal{G}(\mathbf{t}^{(q+1)}, \boldsymbol{\beta}^{(q+1)}, \mathbf{b}^{(q+1)}) - \mathcal{G}(\mathbf{t}^{(q)}, \boldsymbol{\beta}^{(q)}, \mathbf{b}^{(q)})\right| \geq \epsilon$ or $q \leq q_{max}$

IV. Complexity and Convergence Analysis

A. Complexity Analysis

The computational complexity of the proposed resource allocation Algorithm 3 comprises of the complexities involved in solving $(\mathcal{P}4)$, $(\mathcal{P}5)$, and $(\mathcal{P}6)$. Power allocation is carried out by solving $(\mathcal{P}4)$ via sequential convex approximation method. The problem $(\mathcal{P}4.2)$ comprises of ξ=$3N_B$ optimizing variables and ω=$3N_B$+1 constraints and can be solved using via interior point method. The computation complexity is $O\left(I_1\left(\xi^{0.5}(\xi\omega^2+\omega^3)\log(2\xi/\epsilon_q)\right)\right)$ where ϵ_q denotes iteration accuracy and I_1 is the number of iterations required for convergence of the Algorithm 2 [34]. The complexity involved in solving problem $(\mathcal{P}5)$ is C_2=$O\left(I_2(3N_B)^2\right)$ [6], where I_2 denote the number of iterations required for convergence of convex problem $(\mathcal{P}5)$. In $(\mathcal{P}6)$ there are N_B decision variables and $4N_B+1$ constraints, thus computation complexity of linear optimization problem is C_3=$O\left((4N_B+1)N_B^3\right)$ [35]. Therefore, the overall complexity of the joint resource allocation problem is $O\left(I_3(C_1+C_2+C_3)\right)$, where I_3 is the number of iteration required for convergence of Algorithm 3.

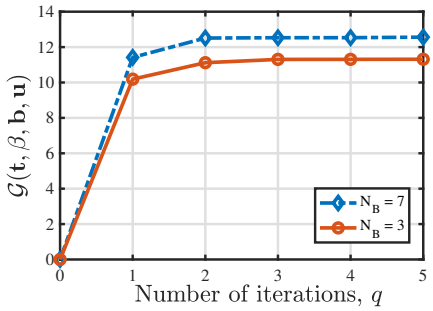

Figure 3: Convergence of the proposed BSC+WET scheme.

B. Convergence Analysis

Let, $\{\mathbf{t}^{(q+1)},\boldsymbol{\beta}^{(q+1)},\mathbf{b}^{(q+1)}\}$ and $\{\mathbf{t}^{(q)},\boldsymbol{\beta}^{(q)},\mathbf{b}^{(q)}\}$ be the feasible solution obtained after $(q+1)^{\text{th}}$ and q^{th} iteration, respectively. The solution set $\left(\mathbf{b}^{(\ell)},\boldsymbol{\zeta}^{(\ell)},\boldsymbol{\varrho}^{(\ell)}\right)$ obtained at the end of the ℓ iteration in Algorithm 2 is also a feasible solution for $\ell+1$ iteration due to $(\hat{C}_4)$ [34]. Therefore Algorithm 2 yield a non decreasing sequence $\mathcal{F}(\mathbf{b}^{(\ell+1)},\boldsymbol{\zeta}^{(\ell+1)},\boldsymbol{\varrho}^{(\ell+1)}) \geq \mathcal{F}(\mathbf{b}^{(\ell)},\boldsymbol{\zeta}^{(\ell)},\boldsymbol{\varrho}^{(\ell)})$. Moreover $\mathcal{F}(\mathbf{b}^{(\ell+1)},\boldsymbol{\zeta}^{(\ell+1)},\boldsymbol{\varrho}^{(\ell+1)})$ is bounded above due to finite transmit power constraint which guarantees the convergence of Algorithm 2. Thus $\mathcal{G}(\mathbf{t}^{(q)},\boldsymbol{\beta}^{(q)},\mathbf{b}^{(q+1)}) \geq \mathcal{G}(\mathbf{t}^{(q)},\boldsymbol{\beta}^{(q)},\mathbf{b}^{(q)})$, and problem $(\mathcal{P}5.1)$ is convex; the optimal solution is obtained by solving the dual problem via subgradient method, thereby $\mathcal{G}(\mathbf{t}^{(q)},\boldsymbol{\beta}^{(q+1)},\mathbf{b}^{(q+1)}) \geq \mathcal{G}(\mathbf{t}^{(q)},\boldsymbol{\beta}^{(q)},\mathbf{b}^{(q+1)})$ holds [6]. $(\mathcal{P}6)$ is linear

in terms of $\mathbf{t}^{(q)}$, therefore $\mathcal{G}(\mathbf{t}^{(q+1)}, \boldsymbol{\beta}^{(q+1)}, \mathbf{b}^{(q+1)}) \geq \mathcal{G}(\mathbf{t}^{(q)}, \boldsymbol{\beta}^{(q+1)}, \mathbf{b}^{(q+1)})$. This proves the non-decreasing nature of $\mathcal{G}(\mathbf{t}, \boldsymbol{\beta}, \mathbf{b})$ over the iterations. Also, $\mathcal{G}(\mathbf{t}, \boldsymbol{\beta}, \mathbf{b})$ is upper bounded due to limited service time. As a result, Algorithm 3 converges within a finite number of iterations, as shown in Fig. 3, yielding a suboptimal set of parameters.

V. Results and Discussion

This section presents the performance results of the proposed UAV-aided monostatic BSC and WET system. These results have been obtained through Monte Carlo simulations conducted in MATLAB. The different parameter values used in the simulations are specified in Table II.

Table II: Simulation parameters and values [5], [27], [36]–[38]

Parameter	Value	Parameter	Value
R_{AOI}	50 m	N	150
a, μ	61.4, 2	N_B^{max}	8
σ_s^2	33.64	b_s	8 bits
P_{com}	18.85 W	T_h	900 s
P_{BSN}	0.1 mW	f_c	28 GHz
h_{UAV}	10 m	σ^2	1×10^{-9}
G_0	10 dBi	κ	40 dB
D_{th}	1 bit	E_{th}	0.32 mW
R_{max}	10 m	$N_x \times N_y$	16×16
K_r	18	P_m	4.927 mW
k_e	0.1	υ, ϑ	$274, 0.29$
δ	0.012	V	10.21 m/s
d_o	0.6	ρ	1.225 Kg/m^3
U_{tip}	120 m/s	v_o	4.03 m/s
s	0.05	A	0.503 m^2
Ω	300 rad/s	R	0.4 m
W	20 N	η_{PA}	27%
P_{DAC}	3.84mW	P_{M}	0.3 mW
P_{LPF}	14 mW	P_{O}	22.5 mW
P_{LNA}	0.5029 mW	P_{ADC}	16.4 mW

A. Energy Efficiency Performance

We first determine the optimal number of beams N_B^* that should be activated at the UAV to serve a cluster and maximize the energy efficiency of the system, as explained in Section

III-B1. Fig. 4 illustrates that there exists an $N_B^* < N_B^{max}$ that maximizes the energy efficiency. The concave nature of the curve is due to the fact that an increase in N_B results in more BSNs being served simultaneously, thereby increasing the total data collected. However, increase in N_B also leads to an increase in RSI on the data beam, resulting in the need for more power to meet the rate constraints. It is notable that the value N_B^* depends on D_{th} and E_{th}. In simulation we have considered BSNs are equipped with DHT-11 sensor which are used to record temperature and humidity values on hourly basis. Per sample BSN consumes 12 mJ [39] and generates total transmit data of 4.5 bytes, which constitutes of 2 bytes of critical device data, namely sampling time, BSN's ID, etc., 2 bytes of sampled data and start bit, end bit, and 2 bits of delimiters in between. Using simple calculation, minimum energy requirement and data collection per unit time is $E_{th} \approx 0.32$ mJ and $D_{\text{th}} \approx 1$ bit. High energy efficiency is due to dual channel coefficients in (11) and E_{th} requirements. The value of N_B^* is utilized in the subsequent simulation studies.

B. Performance Analysis of the Proposed mABC Clustering

Fig. 5 shows the number of clusters N_c formed for different BSN population N. We compare the proposed mABC clustering algorithm, which prioritizes clusters with N_{B_i}=N_B^* BSNs, with two existing BSNs clustering algorithms: modified social group optimization (mSGO) clustering [40] and modified k-means (mk-means) clustering [41]. Here, the mSGO clustering algorithm also employs a hybrid approach, where the search space is reduced based on the given method [42]. In mk-means, the BSNs are initially clustered into N_c=$\lceil N/N_B^* \rceil$ clusters using the k-means clustering. If any cluster violates the constraints, N_c is incremented by one, and the BSNs are re-clustered. This process is repeated until all clusters satisfy the constraints. As observed from Fig. 5, there is a positive correlation between the BSN count and the number of clusters formed. Notably, the mABC algorithm consistently generates the least number of clusters,

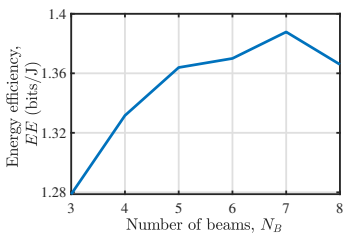

Figure 4: Energy efficiency versus number of beams N_B.

followed by mSGO, while mk-means results in the highest number of clusters. These differences in performance arise from the distinctive strategies employed by each algorithm. Balanced exploration-exploitation approach and adaptiveness of the mABC algorithm based on solution fitness values facilitates swift convergence towards optimal regions within the search space. In contrast, mSGO leans more towards exploitation, which limits its ability to escape local optima. Additionally, mABC and mSGO, with their population-based methodologies, demonstrate greater resilience in accommodating outlying BSNs compared to the more rigid mk-means approach. Consequently, irrespective of the BSN population, the mABC algorithm consistently forms clusters with the minimum number of BSNs, underscoring its efficacy in cluster formation.

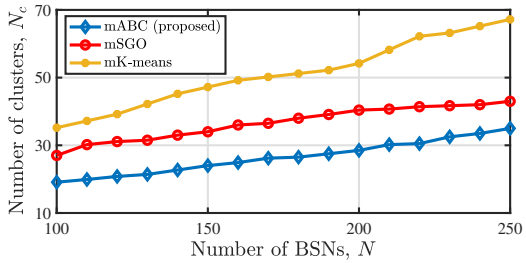

Figure 5: Clustering optimization performance.

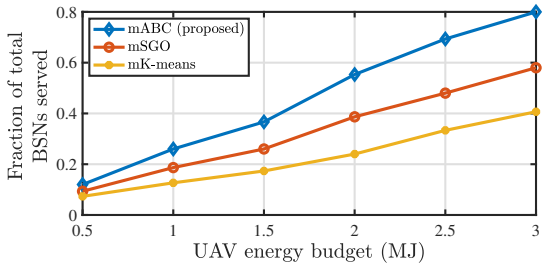

Figure 6: BSN service quality as a function of UAV total energy budget. Total number of BSNs N=150.

To this end, we focused on minimizing N_c by solving ($\mathcal{P}2$) and optimizing the cluster visiting sequence to minimize inter-cluster maneuvering distance. However, these steps did not consider the UAV energy budget. The UAV energy is utilized for BSC, WET, hovering, and inter-cluster movement. It is important to note that there may be situations where the UAV's available energy budget is insufficient to support all N_c clusters. To analyze such scenarios, Fig. 6 illustrates the variation in the fraction of served BSNs as a function of UAV energy budget under different clustering algorithms for a total of N=150 BSNs. With an increase in the energy capacity of the UAV, the ratio of serviced BSNs experiences a consistent rise across all clustering schemes. However, a notable distinction arises in the mABC clustering scheme, where the formation of the least number of clusters (as shown in Fig. 5) leads to a high average BSN count per cluster.

Remark 1. *It can be noticed that the power consumption in UAV hovering and movement exceeds the communication power for BSC and WET operation. Consequently, when the value*

of N_c increases for a given UAV energy budget, BSN count, and deployment scenario, the total hovering time also increases, resulting in a reduced fraction of covered BSNs.

Therefore, with mABC algorithm, which forms the fewest number of clusters among the given N BSNs, the UAV serves a larger proportion of BSNs.

C. Performance Analysis of the Proposed BSC and WET Scheme in a Cluster

Here, we compare the performance of the proposed UAV-aided monostatic BSC and WET scheme over two other closely related works: HTSimOP [15] and HTSeqOP [14]. However, it is important to note that [14], [15] considered IoT nodes operating in half-duplex communication mode. Therefore, for a fair comparison, we incorporate the HTSimOP and HTSeqOP protocols in a BSC framework while employing mABC clustering, which is elaborated as follows.

1) HTSimOP scheme: In this scheme, the τ^{th} time interval is divided into two slots: $\alpha_{E,\bar{D}}\tau$ for WET phase and $(1-\alpha_{E,\bar{D}})\tau$ for BSC phase, where $\alpha_{E,\bar{D}} \in [0,1]$. During the WET phase, all BSNs simultaneously harvest energy from an individual beam. In the BSC phase, all BSNs simultaneously offload the data via a dedicated beam. As a result, due to the simultaneous data offloading by all $N_{B_i}(=N_B)$ BSNs, each data beam experiences RSI and inter-backscatter node interference as well. Moreover, the UAV requires $2N_B$ RF chains for simultaneous data collection and WET operation. Therefore, the total energy consumed by the UAV's transceiver hardware is

$$E_c^{HTSimOP}=\tau\left(2N_B\left(P_{\text{DAC}}+P_{\text{M}}+P_{\text{LPF}}\right)+P_{\text{LO}}+\frac{P_{tot}}{\eta_{\text{PA}}}\right.$$
$$\left.+(1-\alpha_{E,\bar{D}})N_{\text{B}}\left(P_{\text{LNA}}N_{\text{t}}+2P_{\text{ADC}}+P_{\text{LPF}}+P_{\text{M}}\right)\right). \quad (28)$$

2) HTSeqOP scheme: Similar to the HTSimOP scheme, the τ^{th} time interval is divided into two slots: $\alpha_{E,\bar{D}}\tau$ for WET phase and $(1-\alpha_{E,\bar{D}})\tau$ for BSC phase. Unlike HTSimOP, the data from all the BSNs in the BSC phase is collected sequentially, resulting in zero RSI. As data is collected from one BSN at a time, UAV uses two RF chain during the BSC phase and N_B RF chains during the WET phase. Therefore, the total energy consumed by the UAV's transceiver hardware is

$$E_c^{HTSeqOP}=\tau\left(2(\alpha(N_B-1)+1)\left(P_{\text{DAC}}+P_{\text{M}}+P_{\text{LPF}}\right)+P_{\text{LO}}\right.$$
$$\left.+\frac{P_{tot}}{\eta_{\text{PA}}}+(1-\alpha_{E,\bar{D}})\left(P_{\text{LNA}}N_{\text{t}}+2P_{\text{ADC}}+P_{\text{LPF}}+P_{\text{M}}\right)\right). \quad (29)$$

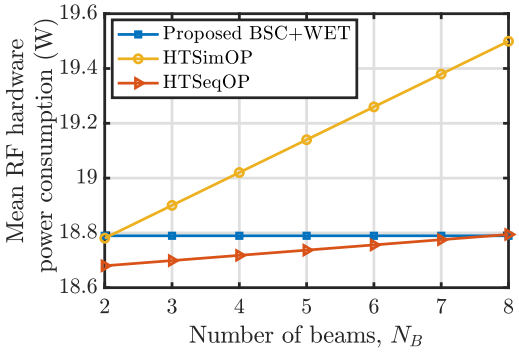

Figure 7: Mean RF hardware power consumption as a function of the number of beams N_B with P_{tot}=5 W.

Fig. 7 illustrates the relationship between the mean RF hardware power consumption and the number of beams. Notably, as the number of beams increases, the mean hardware power consumption consistently remains constant in the proposed scheme. However, it is essential to note that among different schemes considered, HTSimOP stands out with the highest power consumption. On the other hand, HTSeqOP initially exhibits slightly lower power consumption, but this difference becomes less significant as the cluster size increases. This implies that while HTSeqOP may initially offer a slight advantage in terms of hardware power consumption, its impact diminishes as cluster size increases. Following clustering and using the knowledge about the location of BSNs, BSN's cluster association, and CSI, Algorithm 3 is initiated with equal data offloading time, unity backscatter coefficients, and equal power allocation to each BSN.

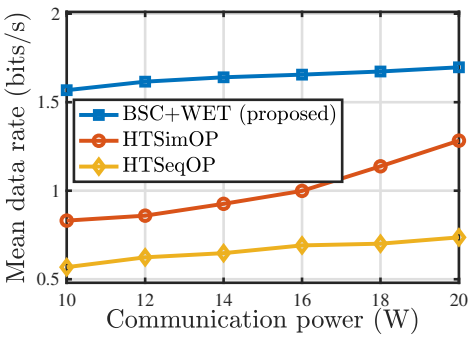

Figure 8: Mean data rate as a function of communication power for BSN cluster size N_c=7, for the same energy harvested in all schemes.

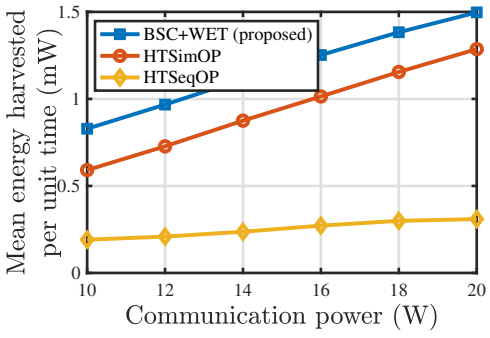

Figure 9: Mean energy harvested as a function of communication power for BSN cluster size N_c=7, for the same data rate in all schemes.

Figs. 8 and 9 provide a comprehensive comparison of performance of the proposed joint

BSC and WET scheme with HTSeqOP and HTSimOP. In Fig. 8, the achievable mean data rate of a cluster are evaluated with respect to the available communication power at the UAV. In the proposed BSC and WET scheme, the data collection and energy harvesting were jointly maximized. For a fair comparison, we maintained the same amount of harvested energy in the HTSeqOP and HTSimOP schemes as achieved in our proposed scheme during each Monte Carlo iteration. Subsequently, the mean collected data rates of HTSimOP and HTSeqOP were maximized accordingly. Similarly, Fig. 9 provides insights into the mean energy harvested per unit time by the BSNs of a cluster for different schemes. For a fair comparison the mean data rate was kept identical across all schemes.

Remark 2. *The results demonstrate that the proposed scheme outperforms HTSimOP in terms of both mean data rate and harvested energy. This improvement can be attributed to the efficient utilization of UAV energy, which would have otherwise been wasted in the RF circuitry of HTSimOP (as shown in Fig. 7). Furthermore, though HTSeqOP, uses less RF power (Fig. 7), collects less data due to its sequential data collection approach during the BSC phase (Fig. 8).*

D. Impact of Scaling Weights on Mean Data Collected and Energy Harvested

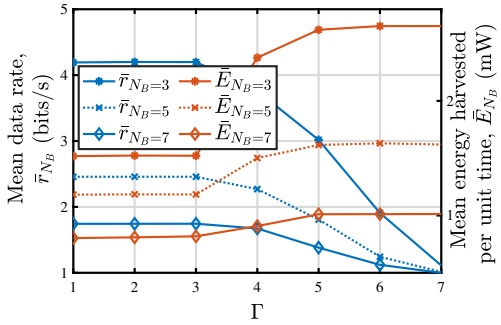

Figure 10: Mean data rate and energy harvesting performance as a function of scaling ratio for different BSN cluster sizes.

So far, we have optimized the resources per cluster considering fixed values of the scaling weights ς_1 and ς_2. However, the priority between collecting additional data and harvesting energy can vary due to spatio-temporal variations. Fig. 10 provides insight into the impact of adjusting the scaling ratio $\Gamma = \log_{10}(\varsigma_2/\varsigma_1)$ on both the mean data rate and harvested energy across different cluster sizes. In general, as the value of Γ increases, there is a noticeable trend for all cluster sizes where the data rate decreases while the energy harvesting rate increases.

This relationship underscores the importance of balancing these competing objectives to achieve optimal performance based on specific system requirements and constraints. when placing a higher priority on energy harvesting (achieved with larger values of Γ), the system tends to allocate more resources towards harvesting energy while meeting the minimum data collection threshold D_{th}. constraints. Conversely, when prioritizing data rate (indicated by lower values of Γ), the BSNs harvest energy close to the minimum energy threshold E_{th} and focus more on maximizing data transmission capabilities. While optimal values of ς_1 and ς_2 can be determined and substituted into the problem $(\mathcal{P}1)$ according to specific system requirements, the precise determination of these values lies beyond the scope of the current study.

E. Total Data Collected and Energy Harvested with N BSNs versus UAV Energy Budget

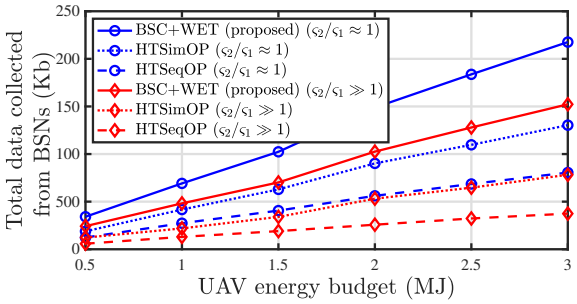

Figure 11: Total data collected by UAV as a function of UAV energy budget with N=150 BSNs.

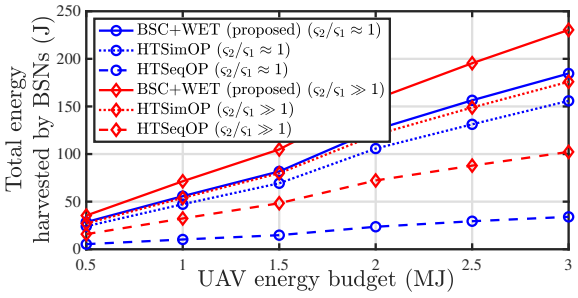

Figure 12: Total energy harvested by BSNs as a function of UAV energy budget with N=150 BSNs.

Fig. 11 shows the total data collected from N BSNs using the proposed joint BSC and WET system, HTSimOP, and HTSeqOP, when BSNs are clustered using mABC algorithm. Here also, for a fair comparison the energy harvested by all schemes is kept the same. As explained in Section V-C, in HTSimOP, due to simultaneous data offloading from all the BSNs in a cluster, there is RSI which degrades the performance of data offloading. In HTSeqOP there is no RSI, since only one BSN is catered at a time during BSC phase. However, zero RSI is achieved at the cost of reduced time availability for data offloading per BSN. Due to this, the overall performance of HTSeqOP deteriorates more in comparison to HTSimOP.

Similarly, Fig. 12 presents the total energy harvested for a given UAV energy budget in the proposed scheme and the benchmark schemes under the condition that the total data collected in all schemes are the same. In Figs. 11 and 12, two contrasting Γ values are considered to capture data-centric optimization and energy-centric optimization. While the data-centric approach yields a higher total data collected, the energy-centric approach results in more harvested energy.

VI. Conclusion and Future Works

This work has presented a UAV-aided joint data collection and charging framework in BSC networks. To remove the dependencies from terrestrial cellular infrastructure, monostatic BSC based architecture has been adopted. The proposed UAV transceiver utilizes a hybrid beamforming architecture with only 3 RF chains, resulting in a reduced RF circuit power consumption. This provides relatively more transmission power under a fixed communication power budget. To improve the UAV energy efficiency, multiple BSNs are served simultaneously instead of sequentially. To deal with the performance trade-off due to residual self interference in full duplex BSC and WET operation, an optimal number of BSNs in a cluster has been computed offline. Accordingly, the BSNs deployed in a region of interest are clustered while considering the desired optimal number of BSNs per cluster and other UAV-based cluster dimension constraints. While serving a particular cluster with a given UAV communication power budget, a joint charging and communication data rate maximization problem has been formulated considering minimum energy harvesting and data rate constraints. Backscatter reflection coefficients, data offloading time, power allocation to BSN has been obtained using alternating optimization approach. Simulation results have demonstrated that the proposed joint BSC and WET scheme exhibits superior performance in terms of mean data rate and harvested energy compared to the competitive benchmarks. Efficient utilization of UAV energy in the proposed scheme provides significantly improved system performance. The presented framework motivates an integrated transceiver design, deployment, and optimal access parameter selection problem, for optimizing the system performance.

Further studies on distributed multi-UAV scenarios for BSC would be of future interest. In addition, exploring heterogeneous powered BSNs with dedicated cluster-head nodes to improve BSC network performance is an interesting direction.

References

[1] F. Guo, F. R. Yu, H. Zhang, X. Li, H. Ji, and V. C. Leung, "Enabling massive IoT toward 6G: A comprehensive survey," *IEEE Internet Things J.*, vol. 8, no. 15, pp. 11 891–11 915, Aug. 2021.

[2] U. S. Toro, K. Wu, and V. C. M. Leung, "Backscatter wireless communications and sensing in green internet of things," *IEEE Trans. Green Commun. Netw.*, vol. 6, no. 1, pp. 37–55, Mar. 2022.

[3] S. Suman, S. Kumar, and S. De, "UAV-assisted RF energy transfer," in *Proc. IEEE Int. Conf. Commun. (ICC)*. IEEE, May 2018, pp. 1–6.

[4] N. Varshney and S. De, "Optimum downlink beamwidth estimation in mmWave communications," *IEEE Trans. Commun.*, vol. 69, no. 1, pp. 544–557, Jan. 2021.

[5] G. Yang, R. Dai, and Y.-C. Liang, "Energy-efficient UAV backscatter communication with joint trajectory design and resource optimization," *IEEE Trans. Wireless Commun.*, vol. 20, no. 2, pp. 926–941, Feb. 2021.

[6] M. Hua, L. Yang, C. Li, Q. Wu, and A. L. Swindlehurst, "Throughput maximization for UAV-aided backscatter communication networks," *IEEE Trans. Commun.*, vol. 68, no. 2, pp. 1254–1270, Feb. 2020.

[7] T. Wang, X. Pang, J. Tang, N. Zhao, X. Zhang, and X. Wang, "Time and energy efficient data collection via UAV," *Sci. China Inf. Sci.*, vol. 65, no. 8, Jul. 2022.

[8] J. Chen and J. Tang, "UAV-assisted data collection for dynamic and heterogeneous wireless sensor networks," *IEEE Wireless Commun. Lett.*, vol. 11, no. 6, pp. 1288–1292, Jun. 2022.

[9] S. Yang, Y. Deng, X. Tang, Y. Ding, and J. Zhou, "Energy efficiency optimization for UAV-assisted backscatter communications," *IEEE Commun. Lett.*, vol. 23, no. 11, pp. 2041–2045, Nov. 2019.

[10] M. Hua, L. Yang, Q. Wu, and A. L. Swindlehurst, "3D UAV trajectory and communication design for simultaneous uplink and downlink transmission," *IEEE Trans. Commun.*, vol. 68, no. 9, pp. 5908–5923, Sep. 2020.

[11] R. Zhang, X. Pang, J. Tang, Y. Chen, N. Zhao, and X. Wang, "Joint location and transmit power optimization for NOMA-UAV networks via updating decoding order," *IEEE Wireless Commun. Lett.*, vol. 10, no. 1, pp. 136–140, Jan. 2021.

[12] C. Zhang, L. Zhang, L. Zhu, T. Zhang, Z. Xiao, and X.-G. Xia, "3D deployment of multiple UAV-mounted base stations for UAV communications," *IEEE Trans. Commun.*, vol. 69, no. 4, pp. 2473–2488, Apr. 2021.

[13] S. Suman, S. Kumar, and S. De, "UAV-assisted RFET: A novel framework for sustainable WSN," *IEEE Trans. Green Commun. Netw.*, vol. 3, no. 4, pp. 1117–1131, Dec. 2019.

[14] K. Lin, O. L. A. López, H. Alves, D. Chapman, N. Metje, G. Zhao, and T. Hao, "Throughput optimization in backscatter-assisted wireless-powered underground sensor networks for smart agriculture," *Internet Things*, vol. 20, p. 100637, Nov. 2022.

[15] W. Feng, J. Tang, N. Zhao, X. Zhang, X. Wang, K.-K. Wong, and J. A. Chambers, "Hybrid beamforming design and resource allocation for UAV-aided wireless-powered mobile edge computing networks with NOMA," *IEEE J. Sel. Areas Commun.*, vol. 39, no. 11, pp. 3271–3286, Nov. 2021.

[16] K. Han and K. Huang, "Wirelessly powered backscatter communication networks: Modeling, coverage, and capacity," *IEEE Trans. Wireless Commun.*, vol. 16, no. 4, pp. 2548–2561, Apr. 2017.

[17] Y. Xu, B. Gu, and D. Li, "Robust energy-efficient optimization for secure wireless-powered backscatter communications with a non-linear EH model," *IEEE Commun. Lett.*, vol. 25, no. 10, pp. 3209–3213, Oct. 2021.

[18] V. Va and R. W. Heath, "Basic relationship between channel coherence time and beamwidth in vehicular channels," in *Proc. IEEE 82nd Veh. Technol. Conf. (VTC2015-Fall)*. IEEE, Sep. 2015, pp. 1–5.

[19] V. Va, J. Choi, and R. W. Heath, "The impact of beamwidth on temporal channel variation in vehicular channels and its implications," *IEEE Trans. Veh. Technol.*, vol. 66, no. 6, pp. 5014–5029, Jun. 2017.

[20] Q. Zhang, W. Saad, and M. Bennis, "Millimeter wave communications with an intelligent reflector: Performance optimization and distributional reinforcement learning," *IEEE Trans. Wireless Commun.*, vol. 21, no. 3, pp. 1836–1850, Mar. 2022.

[21] S. Denno and T. Ohira, "Modified constant modulus algorithm for digital signal processing adaptive antennas with microwave analog beamforming," *IEEE Trans. Antennas Propag.*, vol. 50, no. 6, pp. 850–857, Jun. 2002.

[22] N. Varshney and S. De, "Design optimization for UAV aided sustainable 3D wireless communication at mmwaves," *IEEE Trans. Veh. Technol.*, vol. 72, no. 3, pp. 3274–3287, Mar. 2023.

[23] D. Mishra and E. G. Larsson, "Optimal channel estimation for reciprocity-based backscattering with a full-duplex MIMO reader," *IEEE Trans. Signal Process.*, vol. 67, no. 6, pp. 1662–1677, Mar. 2019.

[24] K. E. Kolodziej, B. T. Perry, and J. S. Herd, "In-band full-duplex technology: Techniques and systems survey," *IEEE Trans. Microw. Theory Tech.*, vol. 67, no. 7, pp. 3025–3041, Jul. 2019.

[25] G. Liu, F. R. Yu, H. Ji, V. C. M. Leung, and X. Li, "In-band full-duplex relaying: A survey, research issues and challenges," *IEEE Commun. Surveys Tuts.*, vol. 17, no. 2, pp. 500–524, 2015.

[26] A. Koc and T. Le-Ngoc, "Full-duplex mmwave massive MIMO systems: A joint hybrid precoding/combining and self-interference cancellation design," *IEEE Open Journal of the Communications Society*, vol. 2, pp. 754–774, 2021.

[27] Y. Zeng, J. Xu, and R. Zhang, "Energy minimization for wireless communication with rotary-wing UAV," *IEEE Trans. Wireless Commun.*, vol. 18, no. 4, pp. 2329–2345, Apr. 2019.

[28] Q. Yue, J. Hu, K. Yang, and C. Huang, "Transceiver design for simultaneous wireless information and power multicast in multi-user mmwave MIMO system," *IEEE Trans. Veh. Technol.*, vol. 69, no. 10, pp. 11 394–11 407, Oct. 2020.

[29] Z. Zhu, M. Ma, G. Sun, W. Hao, P. Liu, Z. Chu, and I. Lee, "Secrecy rate optimization in nonlinear energy harvesting model-based mmwave IoT systems with SWIPT," *IEEE Syst. J.*, vol. 16, no. 4, pp. 5939–5949, Dec. 2022.

[30] S. Wang, M. Xia, K. Huang, and Y.-C. Wu, "Wirelessly powered two-way communication with nonlinear energy harvesting model: Rate regions under fixed and mobile relay," *IEEE Trans. Wireless Commun.*, vol. 16, no. 12, pp. 8190–8204, Dec. 2017.

[31] T. X. Tran, W. Wang, S. Luo, and K. C. Teh, "Nonlinear energy harvesting for millimeter wave networks with large-scale antennas," *IEEE Trans. Veh. Technol.*, vol. 67, no. 10, pp. 9488–9498, Oct. 2018.

[32] C. Voudouris and E. Tsang, "Guided local search and its application to the traveling salesman problem," *Eur. J. Oper. Res.*, vol. 113, no. 2, pp. 469–499, Mar. 1999.

[33] K. Xiong, B. Wang, and K. J. R. Liu, "Rate-energy region of SWIPT for MIMO broadcasting under nonlinear energy harvesting model," *IEEE Trans. Wireless Commun.*, vol. 16, no. 8, pp. 5147–5161, Aug. 2017.

[34] R. Long, Y.-C. Liang, Y. Pei, and E. G. Larsson, "Active reconfigurable intelligent surface-aided wireless communications," *IEEE Trans Wireless Commun.*, vol. 20, no. 8, pp. 4962–4975, Aug. 2021.

[35] S. Boyd and L. Vandenberghe, *Convex optimization*. Cambridge, U.K.: Cambridge Univ. Press, Mar. 2004.

[36] P. Skrimponis, S. Dutta, M. Mezzavilla, S. Rangan, S. H. Mirfarshbafan, C. Studer, J. Buckwalter, and M. Rodwell, "Power consumption analysis for mobile mmwave and sub-THz receivers," in *Proc. 2nd 6G Wireless Summit (6G SUMMIT)*. IEEE, Mar. 2020, pp. 1–5.

[37] L. N. Ribeiro, S. Schwarz, M. Rupp, and A. L. de Almeida, "Energy efficiency of mmwave massive MIMO precoding with low-resolution DACs," *IEEE J. Sel. Topics Signal Process.*, vol. 12, no. 2, pp. 298–312, May 2018.

[38] M. R. Akdeniz, Y. Liu, M. K. Samimi, S. Sun, S. Rangan, T. S. Rappaport, and E. Erkip, "Millimeter wave channel modeling and cellular capacity evaluation," *IEEE J. Sel. Areas Commun.*, vol. 32, no. 6, pp. 1164–1179, Jun. 2014.

[39] S. Ghosh, S. De, S. Chatterjee, and M. Portmann, "Learning-based adaptive sensor selection framework for multi-sensing WSN," *IEEE Sensors J.*, vol. 21, no. 12, pp. 13 551–13 563, Jun. 2021.

[40] S. Satapathy and A. Naik, "Social group optimization (SGO): a new population evolutionary optimization technique," *Complex Intell. Sys.*, vol. 2, no. 3, pp. 173–203, Aug. 2016.

[41] J. A. Hartigan and M. A. Wong, "Algorithm as 136: A k-means clustering algorithm," *J. R. Stat. Soc. Ser. C. Appl. Stat.*, vol. 28, no. 1, pp. 100–108, 1979.

[42] J. Lyu, Y. Zeng, R. Zhang, and T. J. Lim, "Placement optimization of UAV-mounted mobile base stations," *IEEE Commun. Lett.*, vol. 21, no. 3, pp. 604–607, Mar. 2017.